J. Fluid Mech. (1975), *vol.* 69, *part* 4, *pp.* 729–752
Printed in Great Britain

The laminar decay of suddenly blocked channel and pipe flows

By S. WEINBAUM† AND K. H. PARKER
Physiological Flow Studies Unit, Department of Aeronautics, Imperial College, London

(Received 1 October 1974)

This paper is a theoretical investigation of the stable laminar decay of a fully established channel or pipe flow following a sudden blockage such as would be caused by the rapid closure of a valve or imposition of an end wall or gate. The development of the subsequent velocity and pressure fields is examined from the instant the initial pressure wave passes until the final decay of all motion. Three time scales of hydrodynamic interest are identified and the relevant solutions are obtained. The time scales are as follows: (i) a very short time characteristic of the passage of the pressure wave during which the velocity field adjusts inviscidly to the new boundary conditions imposed by the presence of the end wall, (ii) a short diffusion time during which the displacement interaction generated by the diffusion of the primary Rayleigh layer induces a substantial secondary motion with distinct side-wall boundary layers and an inviscid core and (iii) a long diffusion time during which the boundary layers fill the entire channel or pipe and the residual motion then dies out. The secondary flow for short diffusion times is of special interest in that it is an example of an unsteady boundary layer where the external pressure gradient and inviscid outer flow are unknown and determined by the integrated time history of the combined mass flow displacement generated by the primary- and secondary-flow boundary layers. The paper closes with some preliminary comments and experimental observations on decelerating pipe flows.

1. Introduction

The temporal or spatial evolution of fully developed parabolic velocity profiles in channels and pipes has been the subject of a number of classical and recent studies in the fluid-mechanics literature. The temporal evolution of a Poiseuille profile in a long pipe following the application of a constant external pressure gradient is described in Szymanski (1932) and Batchelor (1967). The spatial evolution of a Poiseuille profile in the entrance regions of pipes and channels has been studied by Schlichting (1934), Goldstein (1938), Van Dyke (1970) and Wilson (1971), to mention a few of the more prominent investigations. Interestingly, the inverse problem of bringing a fully established Poiseuille

† Present address: Department of Mechanical Engineering, The City College of The City of New York, New York 10031.

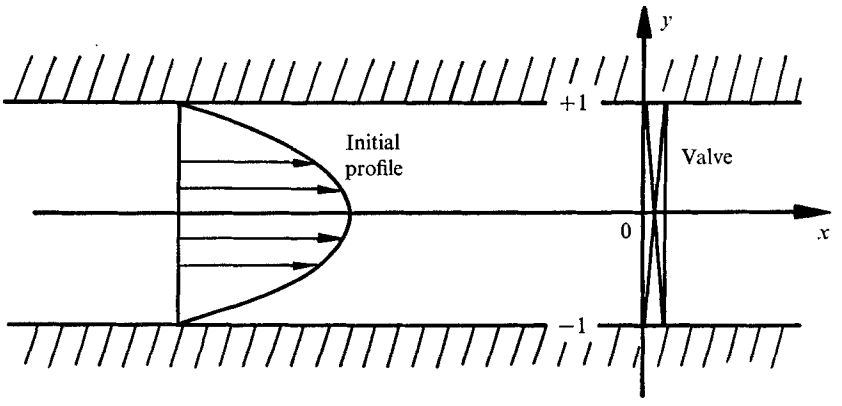

FIGURE 1. Sketch of the channel showing co-ordinate system, location of the valve and initial profile.

flow to rest has not been treated in the literature, to the authors' knowledge, although it is of a rather fundamental nature. In the present investigation we examine the laminar decay of a planar or axisymmetric Poiseuille flow following sudden blockage of a long channel or pipe such as would be produced by the rapid closure of a valve.

Putting aside for the moment the question of stability, the unsteady laminar diffusion problem following the passage of the pressure wave caused by the blockage is considerably more subtle than the starting-flow problem for the pipe or channel flow mentioned above. The sudden imposition of an end wall at $x = 0$ (see sketch in figure 1) imposes the constraint that the integrated volume flux across the channel or pipe must vanish for an incompressible fluid. Because of this constraint, the motion after the passage of the pressure wave is no longer a simple Rayleigh diffusion problem, even far from the end wall, where it is reasonable to assume that the flow is still unidirectional and parallel to the boundaries. If one is to conserve mass with an end wall present, the displacement interaction generated by the diffusion of the primary Rayleigh layer must induce a time-varying streamwise pressure gradient which drives a secondary flow which just balances the volume flow defect of the primary flow. This unsteady secondary flow depends upon the integrated time history of the induced pressure field and one is led to an integral equation of the Volterra type for the unknown interaction pressure gradient. The approximate theoretical solutions obtained show that the secondary flow is an important practical consideration since its amplitude grows until it is of the same order of magnitude as the instantaneous centre-line velocity of the primary flow. Such large changes in the velocity profile are obviously important when considering the laminar stability of the decelerating flow. A major interest of this investigation is to study the development of the secondary flow and its accompanying unsteady boundary layer.

The authors' interest in the present problem is of a physiological nature and arose in connexion with a simple flow-visualization apparatus that was constructed to investigate the mechanism of laminar flow instability in decelerating

pipe flow. The motivation for the experiment is to explain the origin of the turbulence that has been observed during the deceleration phase of flow in the aorta (Seed & Wood 1971; Nerem & Seed 1972). In the experiment the behaviour of dye streaks and hydrogen bubbles is observed after the sudden closure of a solenoid valve at the downstream end of a horizontal straight pipe. For Reynolds numbers, based on diameter and mean velocity before the valve is closed, less than approximately 2000 a stable laminar decay qualitatively similar to that described herein is observed. For higher Reynolds numbers, a periodic streamwise instability which grows and degenerates into turbulence is observed. The present paper provides the background for the theoretical and experimental investigation of the stability of this decelerating pipe flow.

Simple order-of-magnitude analysis suggests that the flow behaviour following the sudden stoppage of a pipe or channel flow is characterized by three different time scales: a very short time R/c, where R is the channel half-height or pipe radius and c is the velocity of sound, characteristic of the passage of the pressure wave; a short diffusion time δ^2/ν, where ν is the kinematic viscosity and δ is a thickness characteristic of the growth of the secondary-flow boundary layer; and a long diffusion time R^2/ν characteristic of the asymptotic decay of the residual motion after the side-wall boundary layers have merged at the centre-line. On the shortest time scale, that of the passage of the pressure wave, one finds that both the convection and diffusion of vorticity are negligible for a flow whose Mach number is $\ll 1$. As a result, the vorticity is essentially frozen in the distribution that existed before the flow stoppage and one must solve a Poisson equation for a rotational inviscid flow subject to the new boundary conditions imposed by the presence of the end wall at $x = 0$. The solution shows that the redistribution of the inviscid velocity field due to end effects is confined to a very small region near the blocked end whose length is of the order of the pipe diameter or channel height and that the flow everywhere else is unidirectional.

The interesting question arises as to whether the mathematical problem is linear or nonlinear. The interaction between the pressure gradient and the displacement of the secondary-flow boundary layer is clearly nonlinear. The governing equations, however, are linear. It appears that the nonlinearity arises from the artificial separation of the secondary flow into a core and a boundary layer on the short diffusion time scale. The location of the edge of the boundary layer becomes a nonlinear function of the induced pressure gradient. If no dichotomy is made between core and boundary layer, the problem remains linear, but as will be shown, more difficult to solve in practice.

Sudden blockage of pipes and channels is a common experience and of obvious practical importance. Previous interest has centred almost exclusively on the inviscid flow problem associated with the propagation of the pressure wave immediately following the obstruction of flow, for example, the propagation of bores in open-channel flow and the so-called 'water hammer' problem in water pipes when a valve is suddenly closed. The subsequent diffusion problem has received little attention and is a rather novel example of the nonlinear interaction that takes place between a secondary boundary layer and a core flow that is itself driven by the displacement interaction of a primary Rayleigh layer.

Nonlinear problems of this nature have heretofore been principally of interest in periodic boundary layers with imbedded Stokes layers driven by free-stream fluctuations, see Stuart (1963, 1972). The present secondary-flow analysis differs from classical unsteady Rayleigh-layer problems (for example, the impulsive motion of a cylinder (Goldstein & Rosenhead 1936) and unsteady stagnation-point flows (Kelly 1962; Tokuda 1970)) in the important respect that the inviscid outer flow is not prescribed. For this reason the study that is probably of greatest relevance to the present problem is the recent analysis by Van Dyke (1970) and Wilson (1971) of steady entry flow in a channel, where the complications due to nonlinear interaction between a core flow and a boundary layer are also present. There is a close analogy between the three time scales in the present problem and three different length scales distinguished by Van Dyke and Wilson in the entrance region of a channel. The singular behaviour near the leading edge of the channel wall on the shortest length scale is analogous to that on the time scale characteristic of the passage of the shock wave. The solution on the intermediate length scale, where the boundary layers on the side wall are separated by an inviscid core, is analogous to the present nonlinear displacement interaction solution for short diffusion times. Finally the problem on the long length scale after the side-wall boundary layers have merged is analogous to the present problem for long diffusion times. The channel entry problem is further complicated by the fact that the governing equations are themselves nonlinear and that the core flow at $x = 0$ depends on the boundary conditions specified on the half-plane $x < 0$ and only approaches the uniform core behaviour assumed by Schlichting (1934) after a distance of the order of the channel height. However, the core velocity in the channel entry problem monotonically approaches its Poiseuille value and the side-wall boundary layers are simple Blasius layers to lowest order. In the present problem, the core velocity of the secondary flow is considerably more complicated, first achieving a maximum on the short diffusion time scale and then undergoing a long decay to zero. Furthermore, the side-wall boundary layers are not simple Rayleigh layers to lowest order because of the non-uniformity of the core flow.

Section 2 describes the inviscid adjustment in the core following the passage of the pressure wave. Sections 3 and 4 describe the solutions to the secondary-flow diffusion interaction problem for channels and pipes respectively and §5 presents the important numerical results.

2. Core motion following passage of pressure wave

In this section we examine the solution for the velocity distribution in the interior of a channel or pipe on the short time scale R/c immediately after the passage of the pressure wave caused by the instantaneous blockage of the flow at the plane $x = 0$. If one introduces the dimensionless variables $t^* = ct/R$, $\boldsymbol{\omega}^* = R\boldsymbol{\omega}/U$, $\mathbf{u}^* = \mathbf{u}/U$ and $\nabla^* = R\nabla$ into the Navier–Stokes vorticity equation one obtains after dropping the asterisks

$$\frac{\partial \boldsymbol{\omega}}{\partial t} - M\nabla \times \mathbf{u} \times \boldsymbol{\omega} = \frac{-M}{Re} \nabla \times \nabla \times \boldsymbol{\omega}, \tag{2.1}$$

where $M = U/c$, $Re = UR/\nu$ and U is the centre-line velocity of the fully established Poiseuille profile just prior to the sudden stoppage of the flow at $x = 0$.

It is evident from (2.1) that if the Mach number $M \ll 1$ and $M/Re \ll 1$ then

$$\partial\boldsymbol{\omega}/\partial t = 0. \tag{2.2}$$

Since the passage of a normal shock wave does not itself generate vorticity (vorticity generation due to wave refraction is a third-order effect for oblique shock waves) one concludes from (2.2) that during the short time interval following the passage of the shock wave the vorticity is essentially frozen in the channel or pipe and has the same distribution as existed with the undisturbed parabolic velocity profile before blockage. Thus, the passage of the shock wave and the introduction of the solid boundary at $x = 0$ cause an almost instantaneous change in the velocity distribution which allows the fluid motion to accommodate its new boundary conditions without changing its vorticity distribution. This change occurs as an impulsive acceleration which is inviscid since viscous diffusion has had no time to act.

In view of these comments the new velocity distribution immediately after the passage of the shock wave satisfies the equation

$$\nabla \times \mathbf{u} = \boldsymbol{\omega}(0^-), \tag{2.3}$$

where $\boldsymbol{\omega}(0^-)$ is the vorticity distribution in the undisturbed flow. The new boundary conditions with the end wall present are

$$\left.\begin{aligned} u &= 0 \quad \text{on} \quad x = 0, \\ v &= 0 \quad \text{on} \quad y = \pm 1 \quad \text{or} \quad r = 1. \end{aligned}\right\} \tag{2.4}$$

The boundary conditions (2.4) are appropriate only for inviscid flow and lead to a solution of (2.3) which permits tangential velocities or, equivalently, infinitesimally thin vortex layers at the walls. The passage of the shock wave, in that it provides an infinite acceleration, is equivalent to an impulsive non-uniform motion of the boundary. The solution of (2.3) and (2.4) thus provides the initial conditions on velocity for the ensuing Rayleigh diffusion, displacement interaction problem, which occurs on a longer time scale. The almost instantaneous change in the velocity field just described may be readily observed using hydrogen-bubble flow-visualization techniques.

2.1. *Initial velocity distribution for planar Poiseuille flow*

For two-dimensional incompressible flow it is convenient to introduce a stream function for the velocity:

$$\mathbf{u} = \nabla \times \psi\mathbf{k}, \tag{2.5}$$

where $\mathbf{k}$ is a unit vector perpendicular to the plane of the motion. The dimensionless undisturbed planar Poiseuille velocity distribution is given by

$$u = 1 - y^2. \tag{2.6}$$

Using (2.5) and (2.6), (2.3) reduces to the Poisson equation

$$\nabla^2\psi = -2y. \tag{2.7}$$

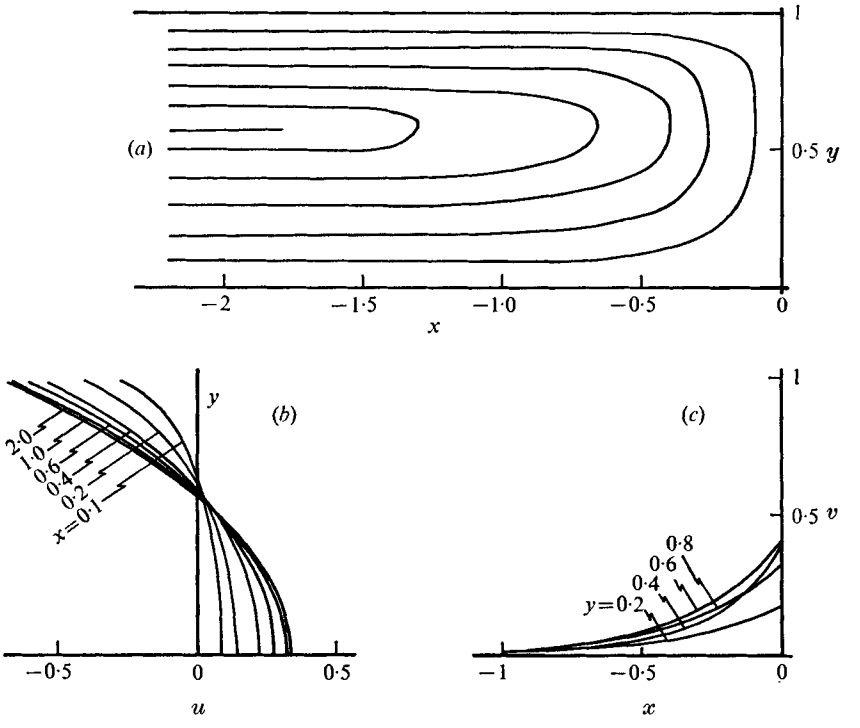

FIGURE 2. Solution near the end wall after the passage of the pressure wave for an initially planar Poiseuille profile. (*a*) Streamlines. (*b*) u profiles at various values of x. (*c*) v profile at various values of y.

The solution of (2.7) which satisfies the boundary conditions (2.4) is obtained by straightforward methods:

$$\psi = \tfrac{1}{3}y(1-y^2)+\frac{4}{\pi^3}\sum_{n=1}^{\infty}\frac{e^{n\pi x}}{n^3}\sin n\pi y. \tag{2.8}$$

The streamlines and the x and y velocity components u and v obtained from (2.5) and (2.8) are shown in figure 2, where the dimensionless x co-ordinate is based on the channel half-height. It is evident from this figure that the vertical velocity component due to end effects vanishes for all practical purposes within a single channel height from the end wall and that the u profile equally rapidly approaches a displaced planar Poiseuille velocity distribution with a dimensionless slip velocity of $-\frac{2}{3}$ at the boundary and a centre-line velocity of $\frac{1}{3}$. Thus, away from the end wall the effect of the pressure wave is simply to decelerate instantaneously the entire velocity profile by an amount equal to the mass-average velocity for the initial undisturbed planar Poiseuille velocity distribution. In this manner the pressure wave instantaneously adjusts the mass-average velocity of the channel flow to zero so as to satisfy the mass-conservation requirement imposed by the end wall.

2.2. *Initial velocity distribution for axisymmetric Poiseuille flow*

For axisymmetric incompressible flow the stream function is defined by

$$\mathbf{u} = \nabla \times \psi \boldsymbol{\phi}, \tag{2.9}$$

where $\boldsymbol{\phi}$ is a unit vector in the azimuthal direction. The dimensionless undisturbed parabolic profile is the same as (2.6) but with y replaced by r, the radial co-ordinate. Using these results in (2.3) one obtains

$$\psi_{rr} + r^{-1}\psi_r - r^{-2}\psi + \psi_{xx} = -2r. \tag{2.10}$$

Equation (2.10) is not of the simple form of (2.7) since the stream function for irrotational axisymmetric flow does not satisfy Laplace's equation. The solution of (2.10) which satisfies the boundary conditions (2.4) can nonetheless be determined by straightforward separation-of-variables methods. This solution is

$$\psi = \frac{r}{4}(1-r^2) + \sum_{n=1}^{\infty} c_n \exp(\mu_n x) J_1(\mu_n r), \tag{2.11}$$

where the μ_n are the zeros of the first-order Bessel function, i.e. $J_1(\mu_n) = 0$, and the constants c_n in the Fourier–Bessel series are given by

$$c_n = 4/\mu_n^3 J_0(\mu_n). \tag{2.12}$$

The solution for the velocity components derived from (2.11) is qualitatively similar to that already shown in figure 2 for the initial velocity distribution following the passage of the shock wave in the channel-flow problem. In figure 3 the development of the centre-line velocity, the slip velocity along the lateral boundary and the decay of the radial velocity component at $r = \frac{1}{2}$ are plotted as functions of dimensionless distance from the end wall and compared with the equivalent results for the channel. The dimensionless centre-line and wall velocities now approach $\frac{1}{2}$ and $-\frac{1}{2}$ respectively. Thus, away from the end wall the parabolic Poiseuille profile for fully established pipe flow is decelerated by half the centre-line velocity after the passage of the shock wave. This is the mean flow velocity for incompressible Poiseuille flow in a pipe.

3. Decay of planar Poiseuille flow

It is evident from the solutions presented in § 2 that fully two-dimensional flow is confined to a region extending a distance of the order of a channel height from the end wall. Outside this region the flow, at least immediately after the passage of the shock wave, is unidirectional. This flow is equivalent to that which would result if the boundaries of the channel were impulsively accelerated in the direction of the original motion to a velocity two-thirds of the original centre-line velocity.

The locally two-dimensional motion near the end wall is of little importance to the flow outside this region and will not be discussed further in this paper. The presence of the wall, however, does have a profound effect on the evolution

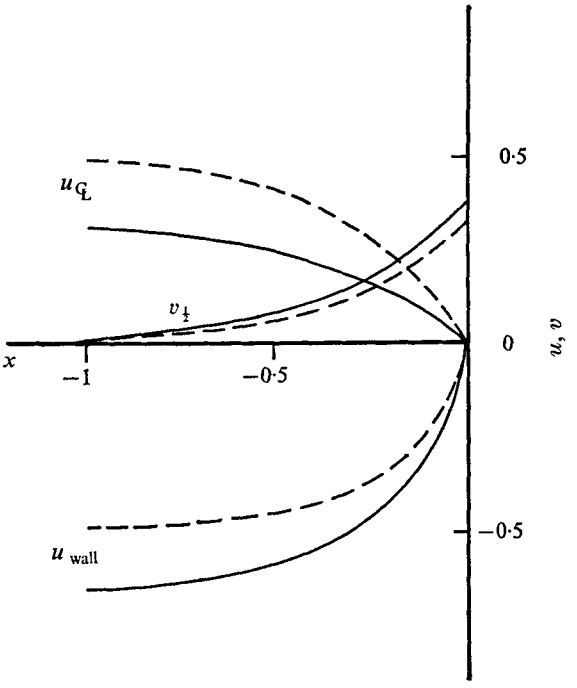

FIGURE 3. Streamwise velocity at the centre-line and at the wall and cross-stream velocity at the midpoint after the passage of the pressure wave. ——, channel; – – –, pipe.

of the flow throughout the rest of the channel. The impenetrability of the end wall and the incompressibility of the fluid require that the integrated volume flux across any cross-section must vanish:

$$\int_0^1 u\,dy = 0. \tag{3.1}$$

The net volume flow resulting from the thickening Rayleigh layer is turned back by the end wall, generating a time-dependent pressure gradient which then becomes the driving force for the secondary motion. The remainder of this section is devoted to developing an approximate solution to this secondary-flow problem which is uniformly valid for all time.

Assuming that the Reynolds number is sufficiently low for a stable unidirectional flow to persist, the dimensionless Navier–Stokes equation governing the ensuing motion is

$$u_t = u_{yy} + \phi'(y). \tag{3.2}$$

Here $\phi'(t) = (-R^2/\mu U)\,dP/dx$ is an unknown time-dependent dimensionless pressure gradient and the time scale has been redefined as $t^* = \nu t/R^2$ so that all the coefficients in (3.2) are unity. The initial and boundary conditions for (3.2) are

$$u = \begin{cases} \frac{1}{3} - y^2 & \text{at} \quad t = 0, \qquad (3.3) \\ 0 & \text{on} \quad y = \pm 1 \quad \text{for} \quad t > 0, \qquad (3.4) \end{cases}$$

where (3.3), the initial condition for the decay of the motion on the diffusion time scale, is obtained from the asymptotic behaviour of (2.8) for large x.

One now seeks a solution of the boundary-value problem posed by (3.2)–(3.4) which satisfies the integral constraint (3.1). The fundamental difference between this problem and the one encountered in classical unsteady boundary-layer analysis for either channel or pipe flow is that the pressure-gradient term $\phi'(t)$ in (3.2) is not prescribed but is an unknown function to be determined by the integral condition (3.1).

The new boundary-value problem just formulated, although involving a mass flow displacement interaction, is still linear since u appears linearly in (3.1). It is convenient therefore, both conceptually and mathematically, to write the solution for u as the sum of two functions w and v representing the primary and induced velocity fields:

$$u(y,t) = w(y,t) + v(y,t). \tag{3.5}$$

The function w, the primary velocity, satisfies the homogeneous equation

$$w_t = w_{yy} \tag{3.6}$$

and the inhomogeneous initial and boundary conditions

$$w = \begin{cases} \frac{1}{3} - y^2 & \text{at} \quad t = 0, \qquad (3.7) \\ 0 \quad \text{on} \quad y = \pm 1 & \text{for} \quad t > 0. \qquad (3.8) \end{cases}$$

One recognizes that this auxiliary boundary-value problem is, except for a constant displacement, simply the Rayleigh diffusion problem that would result if the walls of a channel containing a planar Poiseuille flow were impulsively accelerated to two-thirds of the initial centre-line velocity. The solution to (3.6)–(3.8) is

$$w = \sum_{n=1,3,\ldots}^{\infty} (-1)^{\frac{1}{2}(n-1)} \left(\frac{8}{n\pi}\right) \left(-\frac{1}{3} + \frac{4}{n^2\pi^2}\right) \exp\left(-\left(\frac{n\pi}{2}\right)^2 t\right) \cos\frac{n\pi}{2} y. \tag{3.9}$$

The integral of (3.9) gives the volume flow defect produced by the diffusion of the primary Rayleigh layer:

$$\int_0^1 w\,dy = \sum_{n=1,3,\ldots}^{\infty} \frac{8}{n^2\pi^2} \left(\frac{-4}{n^2\pi^2} + \frac{1}{3}\right) \exp\left(-\left(\frac{n\pi}{2}\right)^2 t\right) = -f(t). \tag{3.10}$$

This volume flow defect is a function of time and will henceforth be referred to as the primary-flow displacement function $f(t)$. Note that $f(t) < 0$ as defined above and the retarded flow near the boundaries is in the $-x$ direction.

The function v in (3.5), the secondary or induced velocity, satisfies the inhomogeneous differential equation and the homogeneous boundary and initial conditions

$$v_t = v_{yy} + \phi'(t), \tag{3.11}$$

$$v = 0 \begin{cases} \text{for all } y \quad \text{at} \quad t = 0, & (3.12) \\ \text{on} \quad y = \pm 1 \quad \text{for} \quad t > 0. & (3.13) \end{cases}$$

Also, from (3.1), (3.5) and (3.10)

$$\int_0^1 v\,dy = f(t). \tag{3.14}$$

Equations (3.11)–(3.14) constitute the boundary-value problem for the unknown function $\phi'(t)$, i.e. the induced pressure gradient that drives the secondary motion.

At first glance it might appear that the simplest procedure for solving (3.11)–(3.14) is to first determine v as a function of ϕ by solving (3.11)–(3.13) and then solve the integral equation for $\phi(t)$ that emerges after substituting this expression for v in (3.14). We shall briefly summarize this procedure and describe the mathematical difficulties inherent in this approach since this provides insight into and the motivation for the boundary-layer approximation procedure finally adopted.

Equations (3.11)–(3.13) can be readily solved using either Duhamel-integral or Laplace-transform methods in which ϕ is treated as an unknown but arbitrary function of time. The desired expression for v is

$$v(y,t) = \phi(t) + \sum_{n=1}^{\infty} 2(-1)^n (n-\tfrac{1}{2})\pi\Phi(n,t)\cos(n-\tfrac{1}{2})\pi y, \tag{3.15}$$

where

$$\Phi(n,t) = \int_0^t \phi(\tau)\exp[-(n-\tfrac{1}{2})^2\pi^2(t-\tau)]\,d\tau.$$

Substituting (3.15) into (3.14), one obtains after performing the y integration

$$\phi(t) = f(t) + 2\sum_{n=1}^{\infty}\int_0^t \phi(\tau)\exp[-(n-\tfrac{1}{2})^2\pi^2(t-\tau)]\,d\tau. \tag{3.16}$$

Equation (3.16) is a linear integral equation of the Volterra type involving an infinite series of integrals containing the unknown function ϕ.

The difficulties encountered in obtaining a uniformly valid solution to (3.16) using analytical methods are formidable. This is due in large measure to the complexity of the primary displacement function $f(t)$, which is plotted in figure 6. One observes that the simple similarity growth characteristic of a Rayleigh layer on a flat plate of infinite extent, that $f(t)$ is proportional to $t^{\frac{1}{2}}$, is valid for only a very small portion of the entire motion, roughly till t is of order 0·01. The interesting feature exhibited by the displacement growth of the primary motion is that $f(t)$ rapidly achieves a maximum and then asymptotically decays to zero on a time scale that is more than an order of magnitude longer than the initial growth period. This behaviour suggests that the primary Rayleigh layer quickly spreads to the centre-line of the channel and then undergoes a much slower decay before all motion subsides. From (3.10) and (3.14) one can attach a simple physical interpretation to $f(t)$: it is the integral average velocity of the secondary flow required to balance the mass flow defect of the primary motion. Thus, at peak amplitude, when $f(t) = 0{\cdot}087$, the mean secondary flow velocity is 26 % of the maximum centre-line velocity of the primary flow. The ratio of the instantaneous centre-line velocities of the secondary and primary flows is significantly greater than this.

The form of (3.16) indicates that ϕ is equal to f plus a boundary-layer-like correction due to the exponential integrals in the infinite sum. For very small times no single exponential integral in (3.16) dominates whereas for large times the function $\phi(\tau)$ in the integrand is far larger than the function $f(\tau)$. This behaviour prevents the solution of (3.16) using standard techniques. The structure of (3.16), however, suggests that an approximate solution of (3.11)–(3.14) might be obtained by dividing the secondary flow into an inviscid core motion and two side-wall boundary layers when the thickness δ of the secondary-flow boundary layers is less than one.

In accord with these remarks we approximate (3.11) in the inviscid core by

$$v_t = \phi'(t), \quad 0 < y < 1-\delta, \tag{3.17}$$

and seek an approximate solution to the full equation (3.11) in the region $1-\delta < y < 1$ using momentum-integral methods. Since $\phi(0) = f(0) = 0$ the solution of (3.17) is

$$\phi(t) = v(t), \quad 0 < y < 1-\delta. \tag{3.18}$$

The function $\phi(t)$ is, therefore, the uniform core velocity of the secondary flow when $\delta < 1$. If one now defines the displacement thickness of the secondary-flow boundary layer as

$$\delta^* = \int_{1-\delta}^{1} \left(1 - \frac{v}{\phi}\right) dy \tag{3.19}$$

the integral condition (3.14) can be written in the compact form

$$\phi - f = \delta^* \phi. \tag{3.20}$$

ϕ thus differs from f, the mean velocity of the primary flow, because of the displacement effect of the secondary-flow boundary layer.

The momentum equation for the secondary-flow boundary layer is obtained by integrating (3.11) across the layer and applying results (3.18) and (3.19). This gives

$$(\delta^* \phi)' = -v_y(1), \tag{3.21}$$

where $v_y(1)$ is the dimensionless shear stress at the top boundary. The value of $v_y(1)$ can be related to δ, ϕ and the pressure gradient ϕ' through the selection of a suitable family of velocity profiles. The arbitrariness of this selection is of course the intrinsic weakness of the momentum-integral method. For the present boundary-layer flow the meaningful velocity boundary conditions are

$$v = 0, \quad v_{yy} = -\phi'(t) \quad \text{on} \quad y = 1, \tag{3.22a, b}$$

$$v = \phi, \quad v_y = v_{yyy} = 0 \quad \text{on} \quad y = 1-\delta. \tag{3.22c–e}$$

Except for the edge condition (3.22e), these are the same as the boundary conditions for the well-known Pohlhausen velocity profile. In the present instance it is logically more consistent to satisfy the condition on the third derivative, since it is an exact description of the boundary-layer equation at the edge of the layer [note that $v_{yt} = 0$ in view of (3.22d)], than to let v_{yy} vanish, which has no rational justification. Also, as $\delta \to 1$, v_{yy} does not vanish whereas v_{yyy} does, from (3.11), in view of the symmetry condition at the centre-line.

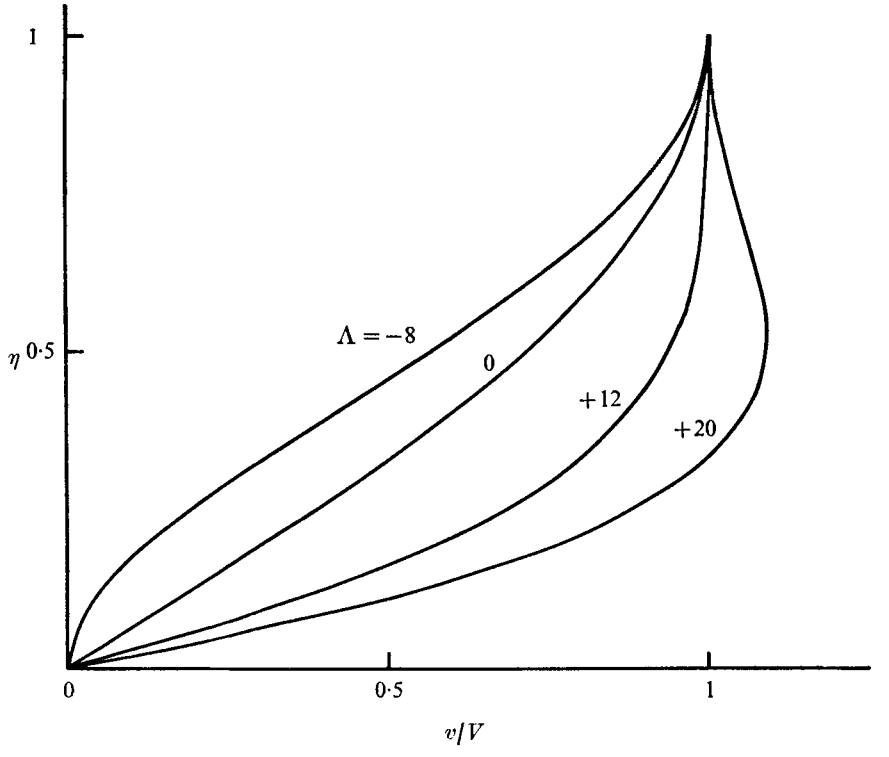

FIGURE 4. Boundary-layer profiles for various values of the shape parameter Λ.

The fourth-order polynomial velocity profile that satisfies the conditions (3.22) is

$$v/\phi = (\tfrac{8}{5}+\tfrac{1}{5}\Lambda)\,\eta - \tfrac{1}{2}\Lambda\eta^2 + (\tfrac{2}{5}\Lambda - \tfrac{4}{5})\,\eta^3 + (\tfrac{1}{5} - \tfrac{1}{10}\Lambda)\,\eta^4, \tag{3.23}$$

where

$$\eta = (1-y)/\delta(t), \quad \Lambda = \delta^2\phi'/\phi. \tag{3.24}$$

This dimensionless velocity profile, when written in terms of the scaled co-ordinate η, is a function of the single parameter Λ defined in (3.24). Profile shapes for typical values of Λ are shown in figure 4. For $\Lambda < -8$ reverse flow occurs whereas for $\Lambda > 12$ a velocity overshoot is obtained in the boundary layer. In contrast to the case for fourth-order Pohlhausen profiles for steady flow, the latter behaviour is meaningful for unsteady boundary layers. As is well appreciated for pipe flows with periodic pressure gradients, the flow near the wall and the flow near the edge of the boundary layer respond differently to a time-varying applied pressure gradient owing to their different inertias.

Given (3.23), the right-hand side of (3.21) may readily be computed. One finds

$$\frac{d}{dt}(\delta^*\phi) = \frac{8}{5}\frac{\phi}{\delta} + \frac{\delta\phi'}{5}. \tag{3.25}$$

The relationship between δ^* and δ is obtained by substituting the expression (3.23) for the velocity profile in (3.19) and integrating:

$$\frac{\delta^*}{\delta} = \tfrac{1}{25}(9 - \tfrac{1}{3}\Lambda). \tag{3.26}$$

Equations (3.20), (3.25) and (3.26) comprise a system of three algebraic and differential relations for the three unknown functions δ, δ^* and ϕ.

The solution of (3.20), (3.25) and (3.26) can be further simplified. Eliminating δ^* gives

$$\phi - f = \tfrac{9}{25}\delta\phi - \tfrac{1}{75}\delta^3\phi', \tag{3.27}$$

$$\phi' - f' = \tfrac{8}{5}\phi/\delta + \tfrac{1}{5}\delta\phi'. \tag{3.28}$$

Each of these equations can now be solved for ϕ' in terms of ϕ, δ and f. Equating these last two results, one can show, after some algebra, that

$$\phi - f = \frac{(27 - 7\delta)\,\delta f - \delta^3 f'}{75 - 42\delta + 7\delta^2}. \tag{3.29}$$

Equation (3.29) is a convenient formula relating ϕ and δ since the function f is known from (3.10). δ and ϕ can be determined as functions of time by solving any two of the three equations (3.27)–(3.29) subject to the initial condition $\phi(0) = 0$. In the present paper a simple marching procedure in which (3.28) was integrated numerically to find the value of ϕ at the next time step was used. This new value of ϕ was then substituted in (3.29) and the resulting cubic equation for δ solved. This numerical integration, however, is not straightforward since (3.28) is singular at the origin and the physically meaningful root for δ must be selected when there is more than one positive real root. These difficulties will be discussed shortly.

An intriguing feature of (3.27) and (3.28) is that they are nonlinear whereas the exact integral equation (3.26) is linear. The nonlinearity is an artificial one and arises because the division of the secondary flow field into an inviscid core with side-wall boundary layers introduces a new unknown, the location δ of the boundary-layer edge, which depends nonlinearly on ϕ. One observes that both (3.27) and (3.28) would be linear if δ were prescribed. When the side-wall boundary layers have diffused to the centre-line $\delta = 1$ of the channel, the problem once again becomes linear. Equations (3.27) and (3.28) are, however, no longer valid since (3.18) does not apply and the formulation must be modified as described in § 3.2.

3.1. *Analytic solution for small diffusion times*

One encounters difficulties in the numerical integration of (3.28) and (3.29) for small times because of the singular nature of both ϕ' and f' as t approaches zero. This problem can be circumvented by developing an analytic solution which is valid for small times.

In accord with the well-known behaviour of impulsive Rayleigh diffusion boundary layers, it is reasonable to assume infinite series solutions for ϕ, f and δ of the form

$$\phi = \phi_0 t^{\frac{1}{2}} + \phi_1 t + \phi_2 t^{\frac{3}{2}} + \ldots, \tag{3.30a}$$

$$f = f_0 t^{\frac{1}{2}} + f_1 t + f_2 t^{\frac{3}{2}} + \ldots, \tag{3.30b}$$

$$\delta = \delta_0 t^{\frac{1}{2}} + \delta_1 t + \delta_2 t^{\frac{3}{2}} + \ldots, \tag{3.30c}$$

where the ϕ_i, f_i and δ_i are unknown constants. Inserting these assumed forms of the solution into (3.27) and (3.28) one obtains the following lowest- and second-order equations relating the various coefficients:

$$\phi_0 - f_0 = 0 \quad \text{at lowest order,} \tag{3.31}$$

$$\left.\begin{aligned} \phi_1 - f_1 &= \tfrac{9}{25}\phi_0\delta_0 - \frac{\delta_0^3 - \phi_0}{150} \qquad (3.32a) \\ \phi_1 - f_1 &= \frac{8}{5}\frac{\phi_0}{\delta_0} + \frac{\delta_0\,\phi_0}{10} \qquad (3.32b) \end{aligned}\right\} \quad \text{at second order.}$$

Thus at lowest order one finds that $\phi_0 = f_0$. This indicates that to lowest order the secondary-flow boundary layer can be neglected and that the core velocity of the secondary flow is the same as the mean velocity defect of the primary Rayleigh layer. It is at second order that the displacement interaction between the secondary-flow core motion and boundary layer first occurs. Equating (3.32a) and (3.32b) one obtains an eigenvalue equation for δ_0:

$$\delta_0^4 - 39\delta_0^2 + 240 = 0. \tag{3.33}$$

The positive real roots of (3.33) are $\delta_0 = 2{\cdot}767$ and $5{\cdot}600$ respectively. The solutions for ϕ_1 and δ_1 are

$$\phi_1 = \frac{16 + \delta_0^2}{10\delta_0} f_0 + f_1, \tag{3.34a}$$

$$\delta_1 = \frac{6(80 - 17\delta_0^2 + \delta_0^4)\,\phi_1}{(210 - 11\delta_0^2)\,\delta_0 f_0}. \tag{3.34b}$$

To $O(t^{\frac{1}{2}})$ the solution for the velocity profile shape factor defined in (3.24) is

$$\Lambda = \tfrac{1}{2}\delta_0^2 + (\delta_0\delta_1 - \tfrac{1}{2}\delta_0^2\phi_1/\phi_0)\,t^{\frac{1}{2}} + \ldots. \tag{3.35}$$

The constants f_0 and f_1 in (3.34) still need to be determined. $f(t)$ is given by (3.10), which is not in a form which can be easily evaluated for small times. There is, however, a well-known procedure for obtaining an approximate solution to this type of diffusion problem which is valid at small times (refer, for instance, to Carslaw & Jaeger 1959). This involves finding the solution of the Laplace transform of the basic equation (3.6) and expanding that solution in a series valid for large values of the transform variable. This series can be inverted term by term to give a solution of the original equation which is valid for small times. The present case is slightly complicated because it is an integral of the solution of the equation which is desired and it is convenient to do the integration before performing the inverse transform. However, the procedure is easily applied, with the result

$$f = \frac{4}{3\sqrt{\pi}}\,t^{\frac{1}{2}} - 2t + \frac{8t^{\frac{3}{2}}}{3\sqrt{\pi}} + \ldots. \tag{3.36}$$

The first two terms of this series are plotted in figure 6 along with the value of f obtained by summing the first fifty terms of the series (3.10). It appears that with only two terms retained the expansion (3.36) is valid for times less than $0{\cdot}01$.

All of the unknown constants in the first two terms of the locally valid series solutions (3.30) have now been determined except for choosing between the two possible values of δ_0 in (3.30). From (3.35) the two possible initial values for the velocity shape factor are $\Lambda(0) = 3{\cdot}83$ and $15{\cdot}67$. The larger value corresponds to a velocity overshoot in the boundary layer, which is physically implausible for a boundary-layer flow whose driving pressure force does not reverse direction. Thus the smaller root, $\delta_0 = 2{\cdot}767$, must be chosen. The small time solutions (3.30) for ϕ and δ are

$$\phi = 1{\cdot}128t^{\frac{1}{2}} + 1{\cdot}035t + O(t^{\frac{3}{2}}), \tag{3.37a}$$

$$\delta = 2{\cdot}767t^{\frac{1}{2}} + 0{\cdot}0251t + O(t^{\frac{3}{2}}). \tag{3.37b}$$

3.2. *Analytic solution for large diffusion times*; $\delta = 1$

Equations (3.27) and (3.28), or (3.20), (3.25) and (3.26), from which they were derived, are no longer valid once $\delta = 1$ since a distinct inviscidly behaving core region no longer exists. The secondary-flow boundary layers have merged at the channel centre-line and the function ϕ no longer corresponds to the uniform core velocity of (3.18). Much of the analysis is, however, easily modified if one lets the channel centre-line velocity V play the role of the core velocity ϕ when $\delta < 1$. Thus, if one replaces ϕ by V in (3.19) and changes the lower limit of integration to zero, one has a continuous definition for δ^*:

$$\delta^* = \int_0^1 \left(1 - \frac{v}{V}\right) dy \quad (\delta = 1). \tag{3.38}$$

The integral condition (3.14) can be written using (3.45) as

$$V - f = V\delta^* \quad (\delta = 1). \tag{3.39}$$

The momentum-integral equation derived from (3.11) that replaces (3.21) is

$$\phi' - f' = -v_y(1) \quad (\delta = 1), \tag{3.40}$$

while the boundary conditions on the velocity profile used to calculate $v_y(1)$ are unchanged from (3.22) except that (3.22*c–e*) are applied at the channel centre-line, where $y = 0$ and $v = V$. The velocity profile (3.23) is therefore the same except that ϕ is replaced by V and η and Λ are redefined as

$$\eta = 1 - y, \quad \Lambda = \phi'/V \quad (\delta = 1). \tag{3.41}$$

Equation (3.40) thus becomes

$$\phi' - f' = \tfrac{1}{5}(8V + \phi') \quad (\delta = 1) \tag{3.42}$$

and δ^* in (3.38) is given by

$$\delta^* = \tfrac{9}{25} - \tfrac{1}{75}\phi'/V. \tag{3.43}$$

Equations (3.39), (3.42) and (3.43) provide three algebraic relations for ϕ, V and δ^*. The solutions for ϕ' and V are

$$\phi' = 3f + \tfrac{6}{5}f', \quad V = \tfrac{3}{2}f - \tfrac{1}{40}f', \tag{3.44), (3.45}$$

while δ^* is given by (3.43) with

$$\Lambda = \phi'/V = (120f + 48f')/(60f - f'). \tag{3.46}$$

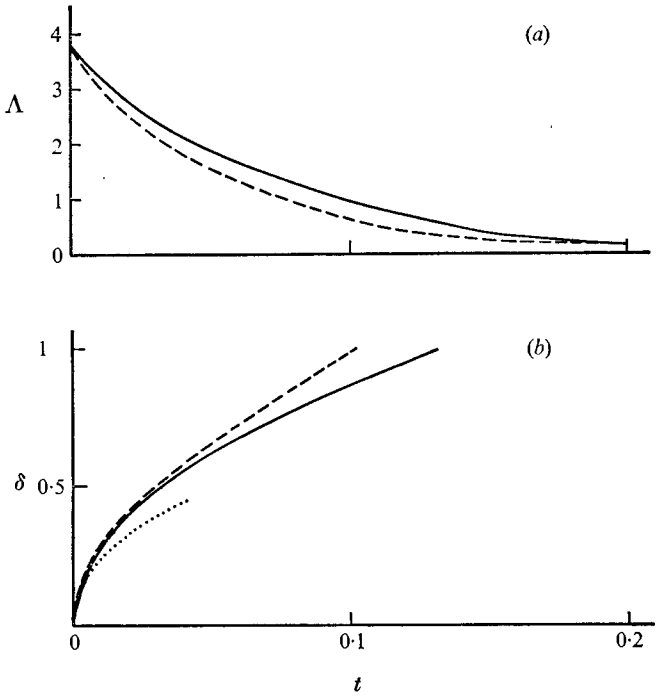

FIGURE 5. (*a*) Calculated shape parameter as a function of time after valve closure. (*b*) Calculated boundary-layer thickness as a function of time. ——, channel; – – –, pipe; · · · ·, analytical solution for small times.

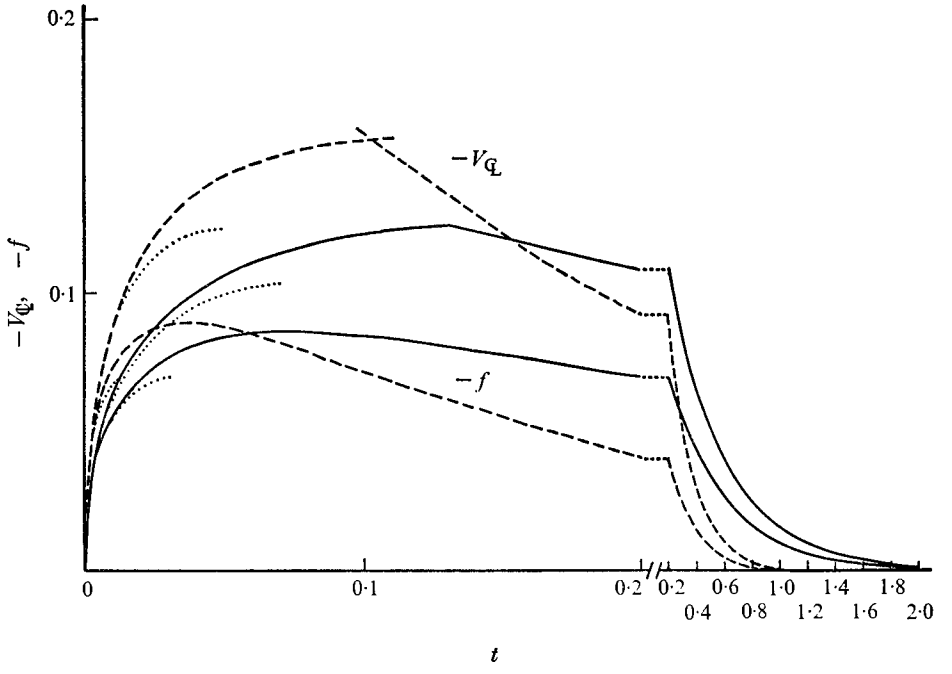

FIGURE 6. Calculated centre-line velocity and primary-flow displacement f as functions of time after valve closure. Note break in time scale. ——, channel; – – –, pipe; · · · ·, analytical solution for small times.

Note that these solutions for the induced pressure gradient ϕ' and the centre-line velocity V are both linear functions of f and its derivative.

The results of the analysis for the secondary velocity are summarized in figures 5 and 6. The boundary-layer thickness δ and shape factor Λ are shown in figure 5. Also plotted are the first two terms of the small time solutions (3.37). The boundary layers grow until they merge at $t = 0{\cdot}131$. The shape factor decreases from its initial value and for large times approaches an asymptote $\Lambda = 0{\cdot}02505$. This asymptote corresponds to the time when all but the lowest mode of the primary velocity (3.9) are damped out and the motion decays in a similar way.

The values of f and V, the centre-line velocity (remember that $V = \phi$ for $\delta < 1$), are shown in figure 6. Note that the time scale along the abscissa has been broken at $t = 0{\cdot}2$ to magnify the detailed structure of the solution for small times. V grows with f for small times but continues to grow after f reaches its peak until the boundary layers merge at $t = 0{\cdot}131$. The maximum value of V, which is the maximum value of the secondary velocity, is 0·126. This is 38 % of the maximum primary velocity at the centre-line and indicates the importance of the secondary velocity in determining the physical velocity u. After the boundary layers merge, V decreases asymptotically to zero.

4. Decay of axisymmetric Poiseuille flow

The flow in a pipe is qualitatively identical to that in a channel. However, because of the geometrical differences, the equations, boundary conditions and hence solutions differ from those presented for planar Poiseuille flow in § 3.

In the region far enough removed from the end wall for the flow to be uni-directional, the governing equation equivalent to equation (3.2) for the planar case is

$$u_t = r^{-1}(ru_r)_r + \phi'(t), \tag{4.1}$$

with the initial and boundary conditions

$$u = \begin{cases} \frac{1}{2} - r^2 & \text{at} \quad t = 0, \qquad (4.2) \\ 0 \quad \text{on} \quad r = 1 & \text{for} \quad t > 0. \qquad (4.3) \end{cases}$$

The velocity field u is again separated into primary- and secondary-flow velocity components w and v as in (3.5). The primary velocity w, which satisfies the homogeneous equation and inhomogeneous boundary conditions derived from (4.2) and (4.3), can be found straightforwardly:

$$w = -\sum_{n=1}^{\infty} \frac{1 - 8/\lambda_n^2}{\lambda_n J_1^2(\lambda_n)} \exp(-\lambda_n^2 t) J_0(\lambda_n r), \tag{4.4}$$

where the λ_n are the ordered zeros of the zero-order Bessel function, i.e.

$$J_0(\lambda_n) = 0.$$

The axisymmetric primary-flow displacement function is defined as

$$f(t) \equiv -2\int_0^1 wr\,dv \tag{4.5}$$

and can be evaluated using (4.4):

$$f(t) = 2\sum_{n=1}^{\infty} \frac{1}{\lambda_n^2}(1 - 8/\lambda_n^2)\exp(-\lambda_n^2 t). \tag{4.6}$$

Equation (4.6) is the axisymmetric counterpart of (3.10).

The secondary velocity v satisfies an inhomogeneous equation and homogeneous boundary conditions which are the axisymmetric equivalents of (3.11)–(3.13) and, in addition, the integral condition

$$2\int_0^1 vr\,dr = f(t). \tag{4.7}$$

When $\delta < 1$, this problem is solved approximately by dividing the secondary flow into a core in which the viscous terms are negligible and a region of thickness $\delta(t)$ near the wall in which viscosity is important. In the core, (4.1) with the viscous term omitted integrates simply to give $v = \phi(t)$. One assumes as in the channel case that the secondary-flow velocity profile in the boundary-layer region near the wall can be represented by a fourth-order polynomial in the scaled co-ordinate $\eta = (1-r)/\delta$. The coefficients of this polynomial are determined by the following conditions imposed on the velocity profile at the wall and at the edge of the boundary layer:

$$\left.\begin{aligned} &v = 0, \quad v_{\eta\eta} - \delta v_\eta = \delta^2\phi'(t) \quad \text{at} \quad \eta = 0, \\ &v = \phi(t), \quad v_\eta = v_{\eta\eta\eta} = 0 \quad \text{at} \quad \eta = 1. \end{aligned}\right\} \tag{4.8}$$

Here $\phi(t)$ is the uniform core velocity at the outer edge of the secondary-flow boundary layer. Conditions (4.8) lead to the profile

$$\frac{v}{\phi} = \frac{8+\Lambda}{5+\delta}\eta + \frac{8\delta - 5\Lambda}{2(5+\delta)}\eta^2 + \frac{-4(1+\delta)+2\Lambda}{5+\delta}\eta^3 + \frac{2(1+\delta)-\Lambda}{2(5+\delta)}\eta^4, \tag{4.9}$$

where Λ is the shape factor $\delta^2\phi'/\phi$. Notice that this profile depends upon two parameters, $\Lambda(t)$ and $\delta(t)$, and is thus more complex than the profile in the channel case, which depended only upon Λ.

Defining the displacement thickness for the axisymmetric secondary-flow boundary layer by

$$\delta^* = \int_{1-\delta}^1 2\left(1 - \frac{v}{\phi}\right) r\,dr, \tag{4.10}$$

relating this definition of δ^* to the primary-flow displacement function $f(t)$,

$$\int_0^{1-\delta^*} 2\phi r\,dr = \int_0^1 2vr\,dr = f(t), \tag{4.11}$$

and evaluating (4.10) using the profile (4.9) leads to the two equations

$$\phi\delta^*(1 - \tfrac{1}{2}\delta^*) = \tfrac{1}{2}(\phi - f), \tag{4.12}$$

$$\delta^*(1 - \tfrac{1}{2}\delta^*) = \delta(1 - \tfrac{1}{2}\delta) - \delta\left[\frac{96 - 45\delta - 11\delta^2 + (2 - \frac{3}{4}\delta)\Lambda}{30(5+\delta)}\right]. \tag{4.13}$$

Integrating the momentum equation across the boundary layer and using (4.9) to evaluate the shear stress at the wall leads to the equation

$$\frac{d}{dt}[(\phi\delta^*(1-\tfrac{1}{2}\delta^*)] = -\frac{8+\Lambda}{5+\delta}\frac{\phi}{\delta}. \tag{4.14}$$

Equations (4.12)–(4.14) are equivalent to equations (3.20), (3.26) and (3.25) for the channel case. δ^* in the former three equations appears only in the combination $\delta^*(1-\frac{1}{2}\delta^*)$ and is thus readily eliminated. The final results equivalent to (3.28) and (3.29) are

$$\phi' - f' = \frac{2\phi}{\delta}\left(\frac{8+\Lambda}{5+\delta}\right), \tag{4.15a}$$

$$\delta^3 + \left(\frac{3\Lambda}{16} - \frac{35}{2}\right)\delta^2 + \left(\frac{15}{4}\left(1-\frac{f}{\phi}\right) - \frac{27}{2} - \frac{\Lambda}{2}\right)\delta + \frac{75}{4}\left(1-\frac{f}{\phi}\right) = 0. \tag{4.15b}$$

The solution of (4.15) valid for $\delta < 1$ is found in a manner that is entirely analogous to the integration of (3.28) and (3.29) described in the last section.

The analytical solution for small times is similar to that presented in §3.1. In fact, after taking into account the difference in the initial velocities at the wall ($w = -\frac{2}{3}$ in the channel, $-\frac{1}{2}$ in the pipe) the lowest-order solutions are identical. The difference in the geometries is reflected in the $O(t)$ terms.

After the core has vanished, $\delta = 1$ and the analysis must be modified as described in §3.2. The velocity profile (4.9) is unchanged except that $\delta = 1$, ϕ is now the axial velocity V and Λ is redefined as ϕ'/V. We give only the final results equivalent to equations (3.44) and (3.45) for the channel-flow case:

$$\phi' = 8f + \tfrac{4}{3}f', \quad V = 2f - \tfrac{1}{24}f', \tag{4.16), (4.17}$$

while δ^* is given by (4.13) with $\delta = 1$ and

$$\Lambda = 32(6f+f')/(48f-f'). \tag{4.18}$$

Equations (4.16) and (4.17) are linear, again illustrating that the nonlinearity exhibited by the solutions for $\delta < 1$ is the result of artificially dividing the problem into two regions: the boundary layer and the core.

The equations for the axisymmetric case have been solved numerically and the results are shown in figures 5 and 6 along with those for the channel. The chief differences are that, as expected, the boundary layers merge at a slightly smaller time, $t = 0{\cdot}103$, and the maximum secondary velocity is considerably higher, 0·156. Similarly, the motion decays more quickly than in a channel.

5. Results and discussion

Having determined the transient behaviour of the secondary-flow velocity profile shape parameter Λ and boundary-layer thickness δ, see figure 5, it is now a simple matter to calculate the time evolution of the actual velocity profile $u(y,t)$. From (3.5), u is the superposition of the primary velocity profile w given by (3.9) or (4.4) and the secondary velocity profile v given by (3.23) or (4.9) for fully developed channel or pipe flow respectively. These results are shown in

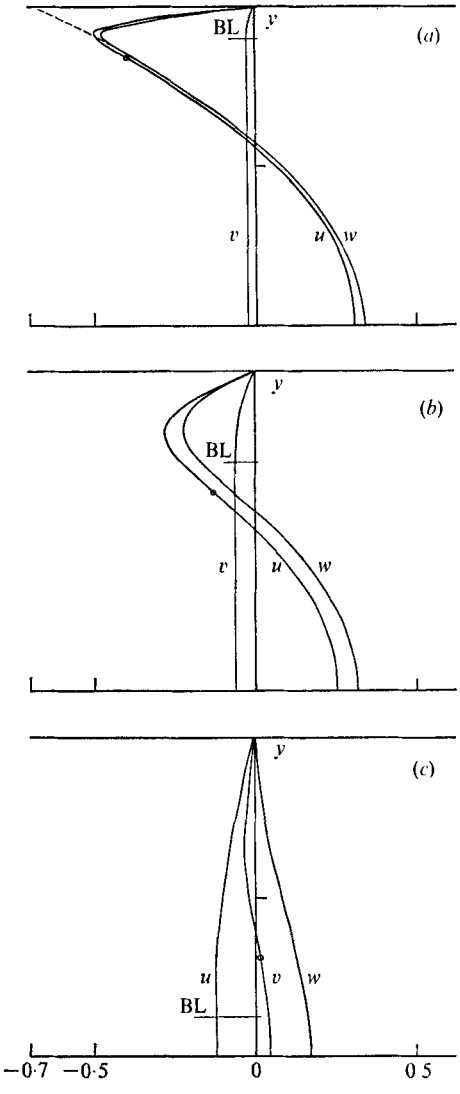

FIGURE 7

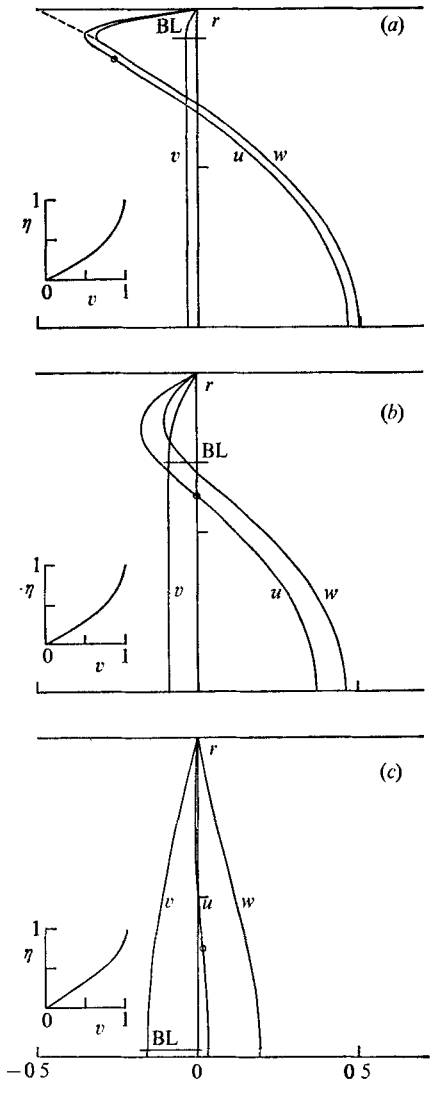

FIGURE 8

FIGURE 7. Velocity profiles in a channel at various times after valve closure. w = primary velocity, v = secondary velocity, u = total velocity. ○, point of inflexion; BL, edge of boundary layer. (*a*) $t = 0{\cdot}001$; – – –, initial profile. (*b*) $t = 0{\cdot}01$. (*c*) $t = 0{\cdot}1$.

FIGURE 8. Velocity profiles in a pipe at various times after valve closure. w = primary velocity, v = secondary velocity, u = total velocity. ○, point of inflexion; BL, edge of boundary layer. Each inset shows the boundary-layer profile. (*a*) $t = 0{\cdot}001$; – – –, initial profile. (*b*) $t = 0{\cdot}01$. (*c*) $t = 0{\cdot}1$.

figures 7 and 8, where the primary- and secondary-flow velocity profiles are shown separately as well as their sum u. Since the normalized axisymmetric secondary-flow boundary-layer profile depends on both δ and Λ from (4.9), the simple one-parameter description shown in figure 4 for channel flow is not sufficient, and the detailed secondary-flow boundary-layer velocity profiles for

the pipe-flow geometry are shown as inserts in figure 8. Also indicated in the figures for both cases are the instantaneous locations of the outer edge of the secondary-flow boundary layer and the point of inflexion in the total velocity profile.

At $t = 0{\cdot}001$ (figures 7*a* and 8*a*) the primary- and secondary-flow velocity boundary layers are confined to a thin region near the wall. The most noticeable deviation from the initial velocity profile is due to the effect of the no-slip condition at the wall on the diffusion of vorticity in the primary velocity profile. The secondary velocity is very small and distributed uniformly throughout almost the entire interior of the channel or pipe. At $t = 0{\cdot}01$ (figures 7*b* and 8*b*) the secondary velocity has increased to roughly 20% of the instantaneous centre-line velocity of the primary velocity profile and the secondary-flow boundary layer has a significant influence on the shape of the total velocity profile. Also, small deviations due to Rayleigh diffusion are noted between the primary and initial velocity profiles near the centre of the channel or pipe. This remark also applies to the secondary flow, where the clear dichotomy assumed in the theory between an inviscid core and a viscous boundary layer is not rigorously valid as δ approaches unity. The abrupt change in slope of the solution for $V_{\mathbb{C}}$ which is observed in figure 6 at the instant that $\delta = 1$ is a manifestation of this shortcoming of the theory. In reality, the effects of diffusion are always present in the core and the transition from the solution for short diffusion times ($\delta < 1$) to that for long diffusion times ($\delta = 1$) is gradual. At $t = 0{\cdot}1$ (figures 7*c* and 8*c*) the secondary-flow boundary layer has nearly filled the entire channel or pipe and the induced and primary velocity profiles are of roughly the same order of magnitude, differing primarily in their shape. For still larger times the w profile is dominated by its lowest-order decaying mode, a parabola, while the v profile approaches a self-similar behaviour in which Λ approaches the value 0·02505. For these large times the accuracy of the solution for the u profiles is strongly dependent on the accuracy of the approximate fourth-order polynomial description of the secondary-flow profile since w and v differ by only a small amount. When v is significantly less than w the inaccuracies in the solution for u introduced by the polynomial approximation for v are obviously less critical. One can find a solution for very large times more accurate than that found here by solving the integral equation (3.15), retaining only the lowest-order term in the infinite series solution for w and then matching at an appropriate time with the present solution. In view of the small amplitude of the residual motion at these very large times this asymptotic analysis is of little practical value and was not attempted.

Since this study was motivated by an interest in the stability of decelerating flows, it seems fitting to conclude with some comments on the stability of the laminar solutions just described. The full stability analysis of this time-varying flow is, of course, very difficult. However, with the guidance of previous stability studies of mathematically related problems and the preliminary experimental results, it is possible to make some superficial observations. A more detailed quasi-steady analysis of the stability of the instantaneous u velocity profiles is currently in progress.

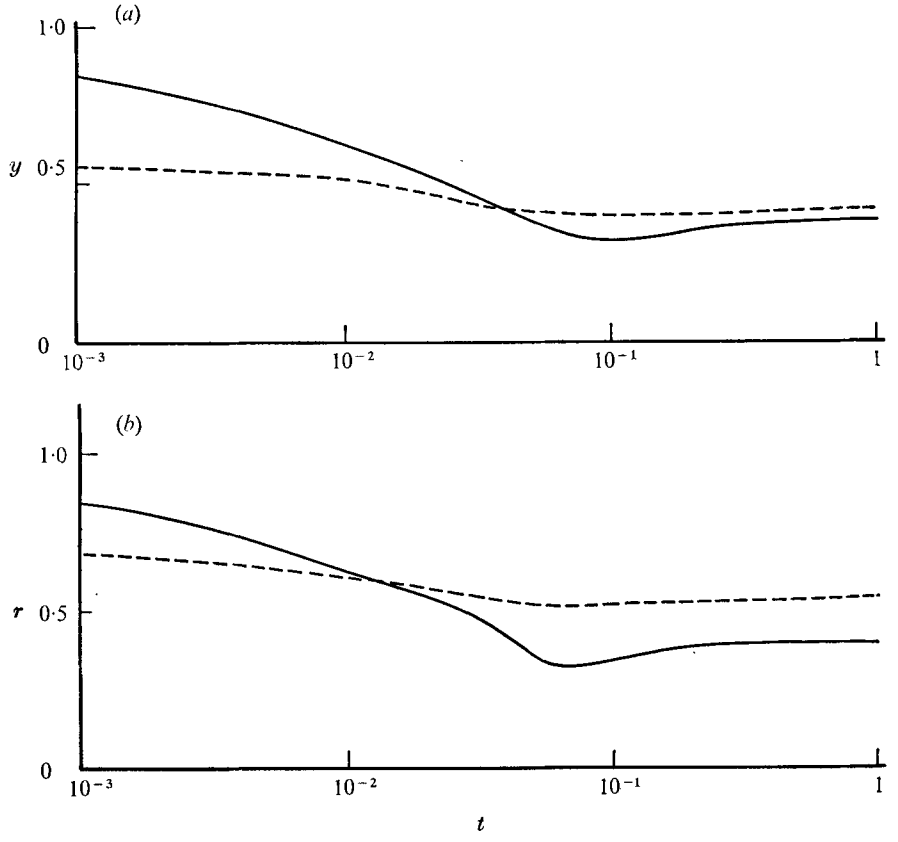

FIGURE 9. Locations of the point of inflexion and the point of zero velocity as functions of time after valve closure. (*a*) Channel. (*b*) Pipe. ——, point of inflexion; – – –, point of zero velocity.

From the point of view of stability, the most notable feature of these flows is the existence of an inflexion point in the u profile. Inflexion points are, of course, points of instability in steady inviscid flows and experience has shown that they are points of particular interest in viscous stability studies. One well-studied stability problem which appears to have special relevance to the present flow is the instability of the Ekman boundary layer on a rotating disk. Theoretical and experimental investigations by Gregory, Stuart & Walker (1955), Faller (1963), Lilly (1966) and others have shown that the dominant mode of laminar instability when the Reynolds number is greater than 125 is a wave which is nearly stationary relative to the surface of the disk and which takes the form of spiral bands of vortex rolls. Theoretical analysis has shown that the instability is of inviscid type and occurs when the point of inflexion in the velocity profile perpendicular to the bands coincides with the point of zero phase velocity.

Preliminary experimental results for a decaying pipe flow indicate that the initial disturbance which is observed is also a standing wave. This observation, coupled with the results for a rotating disk, suggests that the location of the

point of inflexion relative to the point of zero velocity is of particular interest. The locations of these points for both channel and pipe flow are plotted as a function of time in figure 9. It can be seen that the point of zero velocity does not move very far from its initial location ($y = 1/\sqrt{3}$ for a channel, $r = 1/\sqrt{2}$ for a pipe), while the point of inflexion moves rapidly from the wall, its initial location, towards the centre-line. In a pipe, these points coincide at a dimensionless time $t = 0{\cdot}012$. This corresponds to a physical time for the experiment ($R = 2{\cdot}5$ cm, $\nu = 0{\cdot}01$) of approximately 6 s, which is qualitatively the same as the observed time for the appearance of the disturbance. Further experiments are in progress to measure more accurately the wavelength of the stationary wave instability, the time that it takes to appear and the critical Reynolds number for its occurrence.

Finally, although the results of this study apply only to flows with initially Poiseuille profiles, the method can be used equally easily for flows with any initial profile. The initial profile directly affects only the primary velocity w and, hence, the volume flow defect function $f(t)$. Since these quantities are represented by Fourier series, any initial profile which may be Fourier analysed can be easily accommodated. The basic equations for the secondary flow, (3.27) and (3.28) or (4.15a) and (4.15b) for channel or pipe flows, as the case may be, are unchanged, the only modification being that the function $f(t)$ itself is altered. The present analysis is thus readily extended to the flow in the entrance regions of suddenly blocked channels and pipes provided that the Reynolds number is sufficiently high for the streamwise variation of the initial entrance profiles to be small over streamwise distances of the order of the channel height or pipe diameter.

The authors wish to express their appreciation to J. T. Stuart for his many helpful comments and suggestions. S. Weinbaum was partially supported in this research by a Senior Visiting Fellowship from the Scientific Research Council of Great Britain.

REFERENCES

BATCHELOR, G. K. 1967 *An Introduction to Fluid Mechanics*, § 4.3. Cambridge University Press.

CARSLAW, H. S. & JAEGER, J. C. 1959 *Conduction of Heat in Solids*, 2nd edn, § 12.5. Oxford University Press.

FALLER, A. J. 1963 An experimental study of the instability of the laminar Ekman boundary layer. *J. Fluid Mech.* **15**, 560–576.

GOLDSTEIN, S. 1938 *Modern Developments in Fluid Mechanics*, vol. 1, chap. 7. Oxford University Press.

GOLDSTEIN, S. & ROSENHEAD, L. 1936 Boundary layer growth. *Proc. Camb. Phil. Soc.* **32**, 392–401.

GREGORY, N., STUART, J. T. & WALKER, W. S. 1955 On the stability of three-dimensional boundary layers with application to the flow due to a rotating disk. *Phil. Trans.* A **248**, 155–199.

KELLY, R. E. 1962 The final approach to steady, viscous flow near a stagnation point following a change in free stream velocity. *J. Fluid Mech.* **13**, 449–464.

LILLY, D. K. 1966 On the instability of Ekman boundary flow. *J. Atmos. Sci.* **23**, 481–494.

NEREM, R. M. & SEED, W. A. 1972 *In vivo* study of the nature of aortic flow disturbances. *Cardiovasc. Res.* **6**, 1–14.

SCHLICHTING, H. 1934 Laminare Kanaleinlaufströmung. *Z. angew. Math. Mech.* **14**, 368–373.

SEED, W. A. & WOOD, N. B. 1971 Velocity patterns in the aorta. *Cardiovasc. Res.* **5**, 319–330.

STUART, J. T. 1963 In *Laminar Boundary Layers* (ed. L. Rosenhead), chap. 7, pp. 349–408. Oxford: Clarendon Press.

STUART, J. T. 1971 Unsteady boundary layers. *IUTAM Symp. on Unsteady Boundary layers* (1971). Quebec: Laval University Press.

SZYMANSKI, P. 1932 Quelques solutions exactes des équations de l'hydrodynamique du fluide visqueux dans le cas d'un tube cylindrique. *J. Math. Pure Appl.* **11** (9), 67.

TOKUDA, N. 1970 Uniformly convergent series solution for unsteady stagnation flows. In *Fluid Dyn. Trans.*, vol. 5, part 2, pp. 175–191. Warsaw: Polish Acad. Sci.

VAN DYKE, M. 1970 Entry flow in a channel. *J. Fluid Mech.* **44**, 813–823.

WILSON, S. D. R. 1971 Entry flow in a channel. Part 2. *J. Fluid Mech.* **46**, 787–799.